

Pseudo channel: time embedding for motor imagery decoding

MIAO Zhengqing^{1,2*}, ZHAO Meirong¹

1. State Key Laboratory of Precision Measuring Technology and Instruments, Tianjin University, Tianjin 300072, China;

2. Research Group Neuroinformatics, Faculty of Computer Science, University of Vienna, Vienna 1090, Austria

*Corresponding author: MIAO Zhengqing (mzq@tju.edu.cn)

Received: August 1, 2024

Revised: August 23, 2024

Accepted: September 9, 2024

Abstract: Motor imagery (MI) based electroencephalogram (EEG) represents a frontier in enabling direct neural control of external devices and advancing neural rehabilitation. This study introduces a novel time embedding technique, termed traveling-wave based time embedding, utilized as a pseudo channel to enhance the decoding accuracy of MI-EEG signals across various neural network architectures. Unlike traditional neural network methods that fail to account for the temporal dynamics in MI-EEG in individual difference, our approach captures time-related changes for different participants based on a priori knowledge. Through extensive experimentation with multiple participants, we demonstrate that this method not only improves classification accuracy but also exhibits greater adaptability to individual differences compared to position encoding used in Transformer architecture. Significantly, our results reveal that traveling-wave based time embedding crucially enhances decoding accuracy, particularly for participants typically considered “EEG-illiteracy”. As a novel direction in EEG research, the traveling-wave based time embedding not only offers fresh insights for neural network decoding strategies but also expands new avenues for research into attention mechanisms in neuroscience and a deeper understanding of EEG signals.

Key words: motor imagery (MI); pseudo channel; electroencephalogram (EEG); neural networks

0 Introduction

Brain-computer interfaces (BCIs) leveraging motor imagery (MI) enable the direct manipulation of external devices or computer applications through neural activities^[1]. Motor imagery involves the cognitive process of imagining specific movements, such as moving the left or right hand, without actual physical execution. Neuroscience research has established that, despite the absence of overt movement, the electroencephalogram (EEG) signals elicited during motor imagery closely resemble those observed during actual motor execution^[2]. Notably, significant event-related desynchronization (ERD) and synchronization (ERS) are observed in the motor cortex during MI, providing a robust foundation for decoding MI-EEG signals^[3]. Consequently, MI-based BCI systems facilitate motionless control of electronic devices, offering novel communication and interaction avenues for individuals with severe motor impairments^[4]. Furthermore, MI-based BCIs hold considerable promise in rehabilitation medicine, particularly as innovative tools for neural rehabilitation to aid patients in recovering

motor functions following strokes or brain injuries^[5].

EEG, known for its high temporal resolution, is frequently employed to investigate the time-dependent changes in neural electrical signals following specific stimuli. For specific sensory, cognitive, or motor events, the elicited neural electrical signals are referred to as event-related potentials (ERPs), which are measured using EEG. In the case of specific visual stimuli, the corresponding ERPs, which are both time-locked and phase-locked, exhibit distinct ERP components such as P100, N100, P200, N200, and P300. For instance, in the field of cognitive neuroscience, EEG serves as a continuous, real-time physiological measure of cognitive load, capable of detecting subtle fluctuations in cognitive processing that traditional measures may overlook^[6]. However, the EEG signals associated with motor imagery are not phase-locked, making their ERP components less easily identifiable. Additionally, since the neural signals elicited by motor imagery tasks depend on the active participation of the individual and lack a feedback mechanism, it is challenging to pinpoint which segments of the EEG signals during the motor imagery period are most critical. For example, the duration of the imagery period is typically set

between 3 s to 5 s to balance the duration necessary for participants to generate discernible EEG patterns through endogenous cognitive activity^[7-9]. However, individual differences such as attention span, reaction speed, and habitual motor imagery can lead to varying preferences for the duration of this imagery period among participants. Some studies^[2,10] emphasize the necessity to account for these individual differences in EEG frequency bands and timing during the feature extraction phase, highlighting the diversity in EEG data across different moments within the imagery period. In our previous research, we also found that moderately shortening the motor imagery task duration did not significantly reduce the accuracy of MI-EEG decoding^[11]. However, the study did not identify which specific time segments of EEG data were most effective for decoding in different participants. Recent advancements have underscored the pivotal role of artificial neural networks (ANNs) in decoding MI-EEG^[12,13]. While traditional manual feature construction methods have been foundational^[14], techniques employing ANNs automate feature extraction and have significantly enhanced the accuracy of MI-EEG decoding^[11,15]. Nevertheless, these neural network approaches often treat all EEG data within the imagery period as homogeneously significant, which may not reflect the underlying neural dynamics accurately.

Position encoding (or time embedding) might be a method worth considering. Although position encoding is a common technique in natural language processing^[16-18], there is a notable absence of studies exploring the application of position encoding of EEG signals in motor imagery contexts. In natural language processing, positional encoding was introduced to address the issue of dependency between different parts of a sequence. Given the unique characteristics of EEG as a neuroimaging method, particularly its low signal-to-noise ratio, this study aims to explore whether time embedding can be utilized to identify the critical EEG segments that should be emphasized during decoding, especially in decoding methods dominated by artificial neural networks (ANNs). Investigating the role of time embedding in MI-EEG not only offers novel insights for enhancing MI-EEG decoding but also aids in a deeper understanding of the significant differences in EEG signals produced during various stages of motor imagery across different participants. This understanding could provide essential technical support for optimizing motor imagery EEG data collection and advancing the research into individual differences in MI-EEG signals.

To address this, we propose a novel traveling-wave

based time embedding method, integrating it as a pseudo channel in EEG, to assess its impact on the decoding performance of convolutional neural networks for MI-EEG. For comparative analysis, we also employ position encoding method used in the Transformer^[16] architecture. Our investigations span motor imagery datasets with a diverse range of channels, testing across different neural network architectures. Preliminary results suggest that the traveling-wave based time embedding method does not introduce extraneous noise into the MI-EEG signals and potentially enhances feature extraction by neural networks, provided the parameters are suitably chosen. Additionally, findings indicate that traveling-wave based time embedding may be more appropriate for MI-EEG data than the position encoding method employed in Transformer architectures. The time embedding approach proposed in this study holds promise for enhancing the decoding of EEG signals and for deepening our understanding of the underlying neuroscientific mechanisms of EEG activity.

1 Methods

1.1 Heuristic development of time embedding

In the analysis of MI-EEG signals, a common approach involves performing time-frequency analysis on EEG signals collected from different channels. By examining the differences in energy distribution across various frequency bands and time intervals, we can highlight the signal variations among different individuals during motor imagery. As shown in Fig.1, the energy distribution in EEG signals varies across different time periods during the motor imagery task for different participants. The challenge in representing time embedding lies in the fact that the energy distribution differs across channels, making it difficult to incorporate the temporal distribution of EEG energy as prior information into an ANN. However, as depicted in Fig.1, the temporal distribution of energy in MI-EEG resembles wave propagation, with slight differences in the location of peaks (high energy) across different participants or channels. This wave-like phenomenon can also be associated with attention during the motor imagery task. Since it is impossible to directly monitor the participant's level of attention throughout the task, it is reasonable to hypothesize that some participants performed effective motor imagery in the early phase of the task, others in the middle phase, and some in the late phase. This bears a certain similarity to wave propagation.

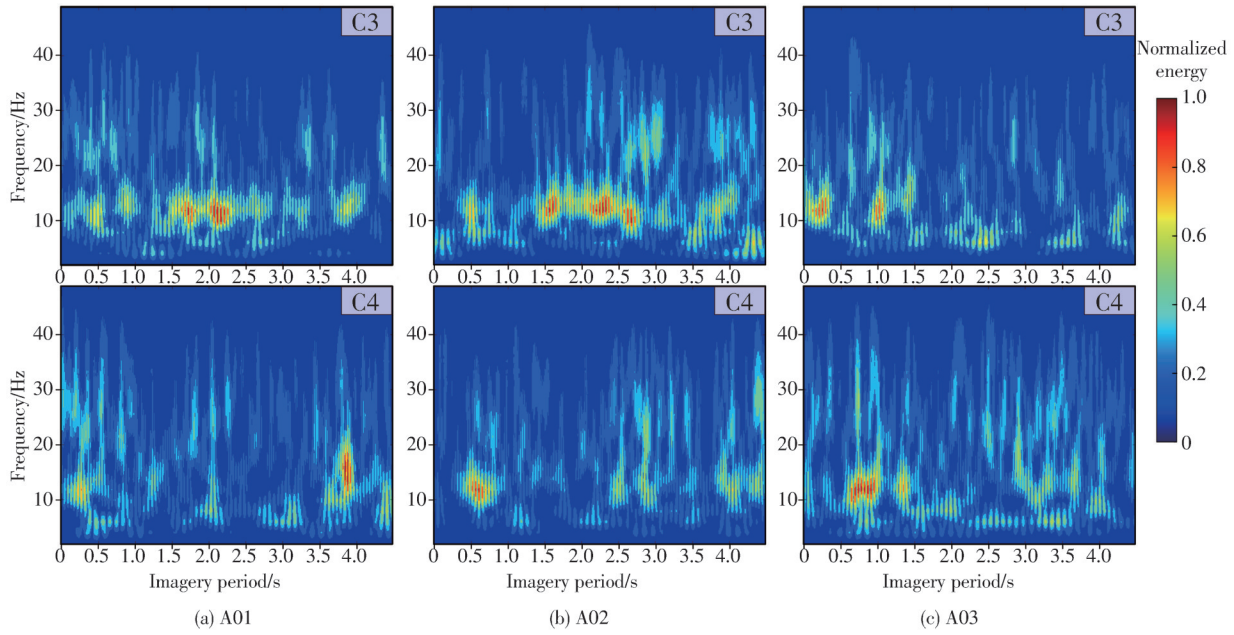


Fig. 1 Normalized energy distribution of EEG signals across different time points and frequency bands during a single trial for various participants. x -axis represents time during the imagery period, with time zero marking the commencement of motor imagery. Energy in the time-frequency plots is normalized.

1.2 Traveling-wave based time embedding

The traveling-wave based time embedding is formulated as

$$y = A \cos\left(\frac{2\pi(x - t)}{\lambda}\right), \quad (1)$$

where A represents the amplitude, corresponding to the

amplitude of the EEG signal, x denotes the position of EEG sampling points during the motor imagery period, t signifies the time offset, and λ indicates the wavelength. As illustrated in Fig.2 (a) and (b), the choice of λ determines the rate of attenuation of the traveling-wave based time embedding within the imagery period—the larger the λ , the slower the attenuation, and vice versa.

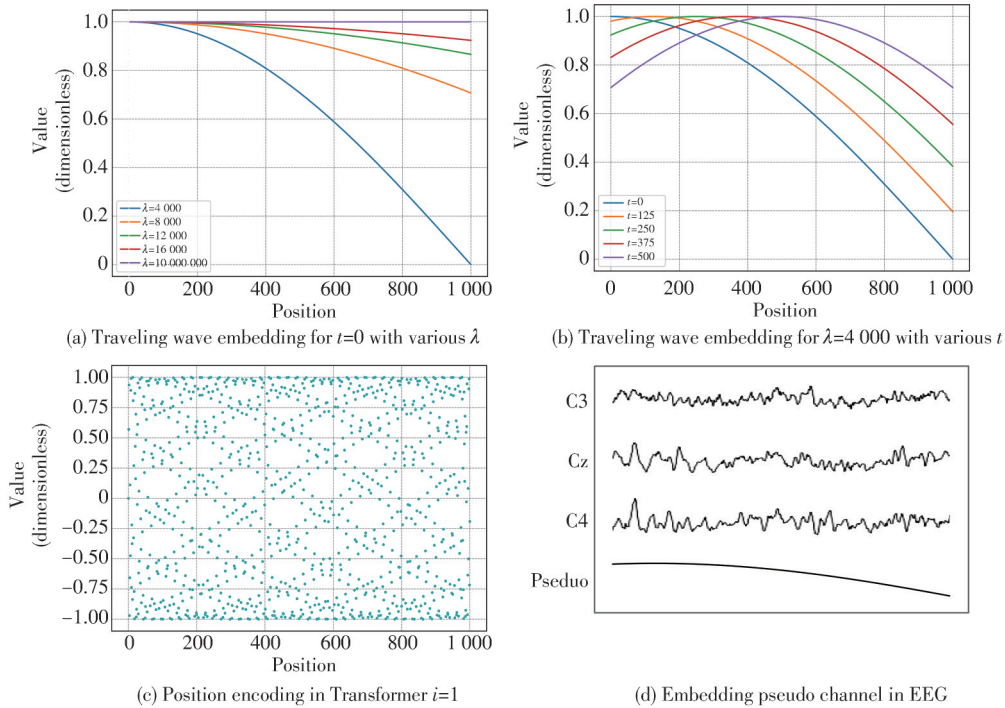


Fig. 2 Visualization of various time-embedding results and their integration into EEG signals. (a) The waveform variations of traveling-wave based time embedding across different values of λ ; (b) The waveform changes of the traveling-wave based time embedding with varying t values; (c) A scatter plot to depict position encoding, highlighting its non-continuous distribution with each position uniquely encoded; (d) The integration of time embedding as a pseudo channel within the EEG.

The value of t determines the instance when the peak of the traveling-wave based time embedding occurs. This method of time embedding parallels the concept of a traveling wave equation, used here to simulate the varying temporal preferences of participants during the motor imagery period.

1.3 Position encoding in Transformer

Position encoding in the Transformer^[16] is achieved by adding a position-dependent vector to the embedding representation of each input element. This allows the model not only to learn from the attributes of the input elements but also to consider their positions within the sequence. The position encoding in a Transformer is defined by

$$PE(pos, 2i) = \sin\left(\frac{pos}{10\,000^{2i/d}}\right), \quad (2)$$

$$PE(pos, 2i + 1) = \cos\left(\frac{pos}{10\,000^{2i/d}}\right), \quad (3)$$

where pos is the position of the element within the sequence, i is the dimension index, and d is the dimensionality of the embedding. This encoding provides unique identifiers for different times within the imagery period by assigning distinct values to even and odd indices. Similarly to the traveling-wave based time embedding, position encoding in the Transformer is also integrated as a pseudo electrode in the preprocessed EEG data.

1.4 Benchmark networks

For this study, we selected two distinctly different artificial neural network architectures as benchmarks: Shallow-ConvNet^[12] (hereafter referred to as ConvNet) and EEGNet^[13]. In ConvNet, the feature extraction network comprises a temporal convolution layer and a spatial convolution layer. In contrast, EEGNet includes an additional temporal convolution layer, with convolution layers that employ sparse connections. Furthermore, both ConvNet and EEGNet utilize kernel sizes in their spatial domain convolutions that match the number of EEG channels, effectively performing a full-connection operation. As indicated in the research by Ref. [19], such full-connection operations can learn the positional attributes of the input data, suggesting that the embedded pseudo electrodes can play a functional role during feature extraction and classification.

2 Datasets

The protocol for collecting motor imagery EEG

signals is highly standardized, involving sequential stages: fixation cross, cue signal, imagery period, and rest (as illustrated in Fig. 3). EEG data acquired in the imagery period are predominantly utilized for pattern recognition and classification tasks^[20]. The time embedding methods proposed in the paper are also applied in imagery period. The EEG datasets used in this study also follow this protocol.

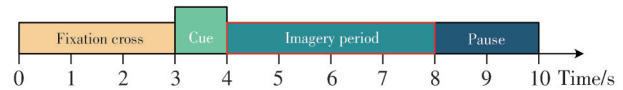


Fig. 3 Typical EEG data collection process during motor imagery trials, illustrating the use of EEG signals acquired during the motor imagery period for decoding.

2.1 BCI4-2A dataset

In the BCI4-2A dataset^[21], EEG data were collected from nine healthy participants (ID A01 – A09) using the international 10 – 20 system, with 22 EEG channels recorded at a sampling rate of 250 Hz. The data collection was performed using a BrainAmp MR plus amplifier and Ag/AgCl electrodes, and the signals were bandpass filtered between 0.5 Hz and 100 Hz, with a notch filter at 50 Hz to remove line noise. Participants performed four motor imagery tasks: imagining movements of the left hand, right hand, both feet, and tongue. The data were collected in two separate sessions, each containing 288 trials (72 trials per task), with visual cues indicating the start of each motor imagery task. The data from the first session were designated for training, while the second session was reserved for testing. The EEG data were labeled based on the type of motor imagery performed, with labels indicating the corresponding class (left hand, right hand, both feet, tongue) provided for each trial.

It is noteworthy that in the original ConvNet paper, the authors utilized EEG data from both the imagery period and the 0.5 s preceding it for decoding. However, our previous work^[11] demonstrated that, with appropriate preprocessing methods, better performance can be achieved by using only the EEG data within the imagery period. This approach is therefore adopted in the current study.

2.2 BCI4-2B dataset

In the BCI4-2B dataset^[22], EEG data were collected from nine healthy, right-handed participants (ID B01 – B09) using three bipolar EEG electrodes (C3, Cz, and C4) at a sampling rate of 250 Hz. The recordings were made using a BrainAmp MR plus amplifier with a

dynamic range of $\pm 100 \mu\text{V}$ for the screening sessions and $\pm 50 \mu\text{V}$ for the feedback sessions. The EEG signals were bandpass filtered between 0.5 Hz and 100 Hz, with a 50 Hz notch filter applied to remove line noise. Participants performed two motor imagery tasks: imagining movements of the left and right hands. Each session consisted of multiple runs, with each run comprising 20 trials per task, resulting in 120 trials per session. The data were labeled based on the motor imagery task being performed, with corresponding class labels (left hand or right hand) provided for each trial. For the purposes of this study, the data from the first three sessions were used for training, while the last two sessions were reserved for testing, as described by Ref. [23]. Only the EEG data recorded during the imagery period were extracted for decoding in this study.

3 Experimental settings

3.1 Data preprocessing

The preprocessing methods used in this paper continue from those employed in our previous work^[24] on motor imagery preprocessing. This involves a [4, 38] Hz 200-order Blackman window bandpass filter, data normalization, and Euclidean spatial alignment. Interested readers may refer to Refs. [15, 24] for more details.

3.2 Experimental environment and parameters

All experiments were conducted on a high-

performance workstation equipped with an Intel Xeon (R) Gold 5117 CPU and an Nvidia Tesla V100 GPU, using the PyTorch framework. The training process employed minibatches of size 32. To ensure fair comparisons across different experimental methods, a unified random seed was used in all experiments to guarantee the repeatability of the experiments. Furthermore, all artificial neural networks were trained for 300 epochs, ensuring consistency.

Besides accuracy(%), the kappa value are also employed as a key evaluation metric in this study to assess the performance of the models.

$$\kappa = \frac{acc - p_0}{1 - p_0}, \quad (4)$$

where acc is the accuracy of model testing, and p_0 is the random level accuracy. The kappa statistic provides a measure of agreement between the model's predictions and the true labels, adjusting for the possibility of chance agreements.

4 Results

The traveling-wave based time embedding technique utilizes two hyperparameters, t and λ . In our experiments, the values for t were explored within the set {0, 125, 250, 375, 500}, and for λ within {4 000, 8 000, 12 000, 16 000, 1 000 000}. As participants exhibit different sensitivities to various hyperparameter combinations, Tables 1 and 2 respectively display the representative hyperparameter search results under two distinct neural network architectures.

Table 1 Binary classification performance of different algorithms on BCI4-2A

Method	Accuracy/%									mean(kappa) \pm std	P-value
	A01	A02	A03	A04	A05	A06	A07	A08	A09		
C_Benchmark	89.2	66.3	94.1	83.7	69.1	58.7	96.5	91.3	87.5	81.8(0.757) \pm 13.6	0.017
C_Transformer	88.9	66.3	92.4	83.3	70.1	59.7	96.5	88.5	88.2	81.6(0.755) \pm 12.9	0.012
C_ $t375 \lambda 16000$	89.6	66.7	95.5	85.8	63.9	65.6	96.2	89.2	87.2	82.2(0.763) \pm 13.1	0.012
C_TravelingWave	92.4	68.1	95.5	87.5	71.5	66.0	96.5	91.0	91.0	84.4(0.792) \pm 12.3	—
E_Benchmark	79.5	68.8	83.3	52.4	65.3	60.1	88.6	81.3	86.8	74.0(0.653) \pm 12.8	0.129
E_Transformer	75.0	60.4	95.5	56.9	58.0	57.3	83.0	82.3	85.4	72.6(0.635) \pm 14.7	0.004
E_ $t125 \lambda 16000$	79.9	63.5	93.4	65.3	58.3	56.9	87.5	80.2	87.2	74.7(0.663) \pm 13.8	0.004
E_TravelingWave	82.3	68.1	95.8	69.1	61.8	59.0	92.4	83.7	87.9	77.8(0.704) \pm 13.6	—

Note: “P-value” indicates the Wilcoxon signed-rank test results, comparing the best performing traveling-wave based time embedding configuration to others within the same ANN. In the “Method” column, ‘C’ denotes the abbreviation for ConvNet, while ‘E’ represents the abbreviation for EEGNet. “_Benchmark” refers to ANNs that do not include any form of time embedding, serving as control models. “Transformer” represents ANNs that incorporate classical position encoding, as utilized in Transformer models. “_ $t375 \lambda 16000$ ” identifies a specific hyperparameter set in the traveling-wave based time embedding that demonstrated the most effective generalization across participants. “_TravelingWave” marks the configuration under the traveling-wave based time embedding that yielded the highest performance for the participant.

One set of results shows the best classification performance for different participants under various hyperparameter combinations, and the other illustrates

the generalizability of a specific hyperparameter set within the traveling-wave based time embedding. The former set demonstrates the variation in participant

performance following the integration of the traveling-wave based time embedding, while the latter reflects the method’s generalization across different participants. These tables also compare the outcomes against networks without any encoding and those utilizing classic position encoding from the Transformer architecture. To

accurately reflect the impact of different hyperparameters in the traveling-wave based embedding on decoding accuracy, we further illustrate these differences using a violin plot in Fig.4 and a heatmap in Fig.5, which details the generalization of different hyperparameter combinations across participants.

Table 2 Binary classification performance (% for accuracy) of different algorithms on BCI4-2B

Method	Accuracy/%									mean(kappa) \pm std	P-value
	B01	B02	B03	B04	B05	B06	B07	B08	B09		
C_Benchmark	80.9	56.1	59.7	97.5	90.3	89.4	82.2	92.2	87.5	81.8(0.636) \pm 14.4	0.359
C_Transformer	76.9	61.4	66.9	97.5	91.6	87.5	82.8	91.3	87.5	82.6(0.652) \pm 12.0	0.129
C_ $t125 \lambda4000$	79.7	62.1	70.0	96.9	92.5	83.1	84.4	90.3	84.7	82.6(0.652) \pm 10.9	0.017
C_TravelingWave	79.7	63.6	72.5	97.8	92.5	86.3	85.6	91.9	86.3	84.0(0.680) \pm 10.6	—
E_Benchmark	80.0	60.0	70.6	97.8	93.8	90.0	86.6	92.8	91.9	84.8(0.696) \pm 12.4	0.012
E_Transformer	81.9	62.1	69.4	97.5	92.5	85.3	82.8	93.1	91.9	84.1(0.682) \pm 11.7	0.012
E_ $t250 \lambda4000$	80.9	64.6	74.4	97.8	94.1	87.2	85.9	94.1	90.3	85.5(0.710) \pm 10.6	0.004
E_TravelingWave	83.1	68.2	75.3	98.1	95.3	99.1	87.5	95.3	91.3	88.1(0.762) \pm 10.7	—

Note: “P-value” indicates the Wilcoxon signed-rank test results, comparing the best performing traveling-wave based time embedding configuration to others within the same neural network architecture. In the “Method” column, ‘C’ denotes the abbreviation for ConvNet, while ‘E’ represents the abbreviation for EEGNet. “_Benchmark” refers to ANNs that do not include any form of time embedding, serving as control models. “_Transformer” represents ANNs that incorporate classical position encoding, as utilized in Transformer models. “_ $t125 \lambda4000$ ” identifies a specific hyperparameter set in the traveling-wave based time embedding that demonstrated the most effective generalization across participants. “_TravelingWave” marks the configuration under the traveling-wave based time embedding that yielded the highest performance for the participant.

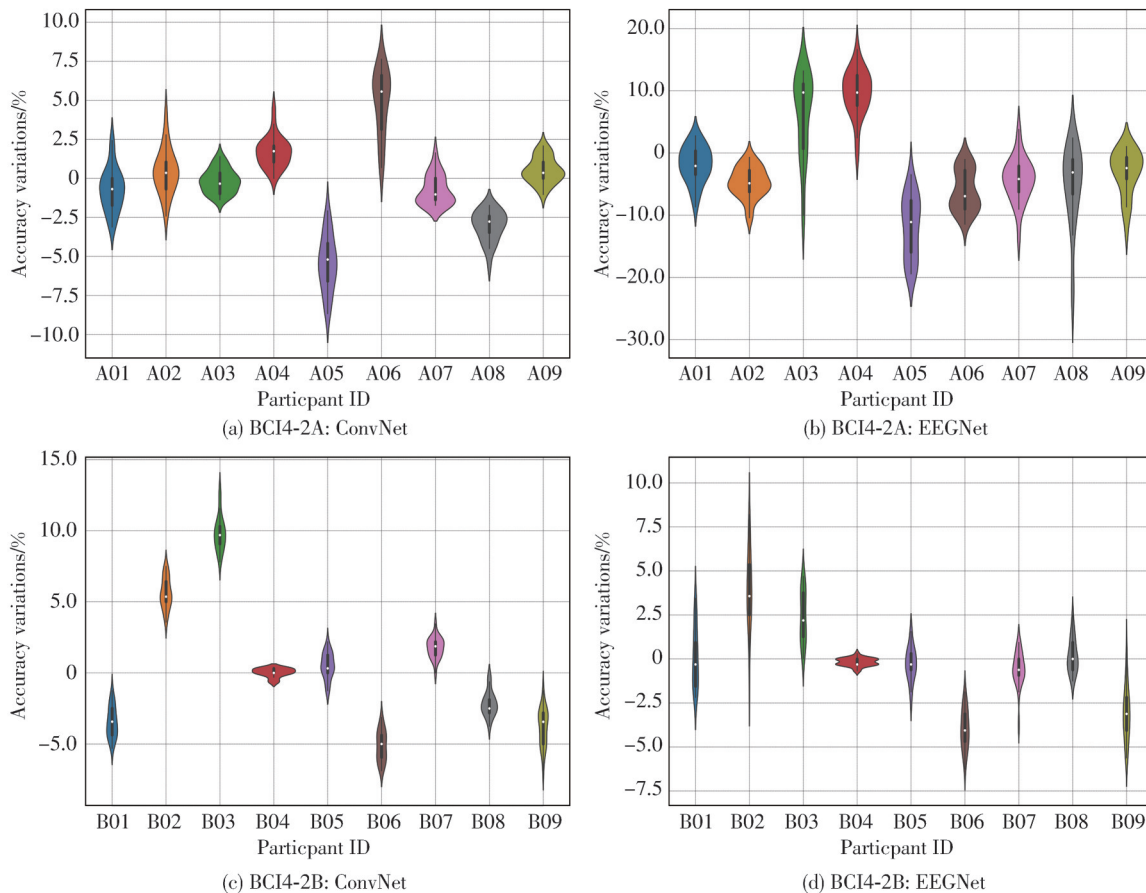


Fig. 4 Variations in decoding accuracy across participants under different hyperparameters of traveling-wave based time embedding compared to benchmark networks. Positive values on the vertical axis indicate higher decoding accuracy compared to the benchmark network, whereas negative values signify lower decoding accuracy than the benchmark network.

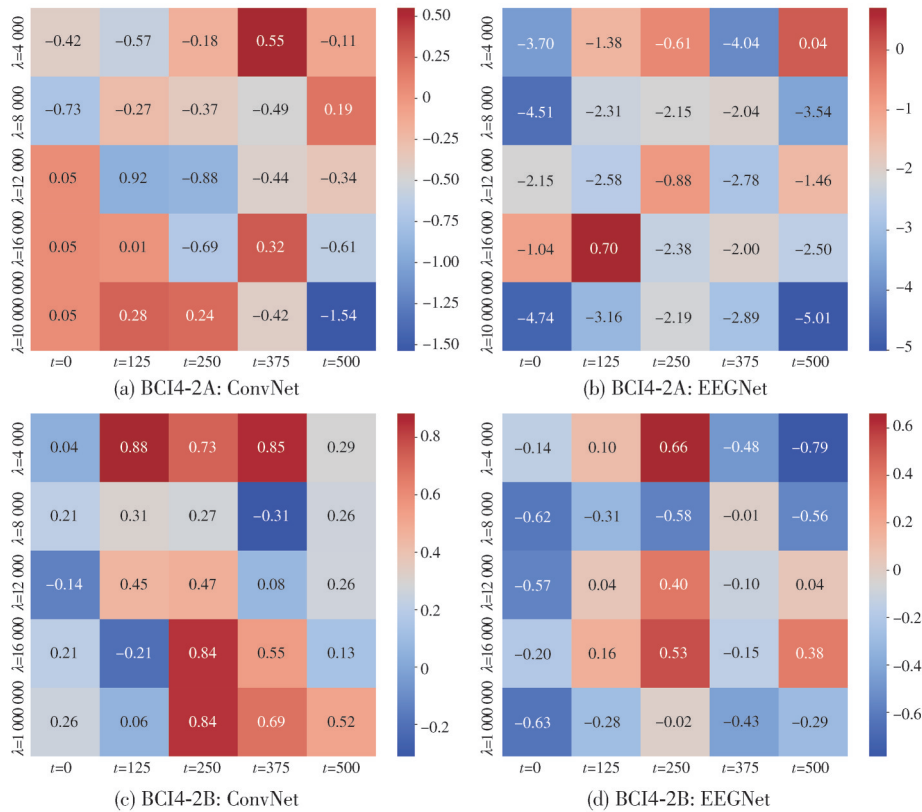


Fig. 5 Average accuracy variations (across all participants) by parameter combinations in traveling-wave based time embedding. Positive values on the vertical axis indicate higher decoding accuracy compared to the benchmark network, whereas negative values signify lower decoding accuracy than the benchmark network.

4.1 Results for BCI4-2A dataset

Table 1 presents the performance of two time encoding methods across two neural network architectures on the BCI4-2A dataset. It can be observed that for both the ConvNet and EEGNet architectures, traveling-wave based time embedding enhances the classification accuracy of the benchmark network to a certain extent. In contrast, position encoding in Transformer does not improve, and in some cases decreases, the classification performance. This suggests that CNN can extract useful information from the time embedding, which also functions as a pseudo channel, and that the traveling-wave based time embedding is more suited to EEG signals than the position encoding method used in Transformer. Furthermore, time embedding strategies reveal differences among participants as well as between the neural network architectures. For instance, in the EEGNet architecture, traveling-wave based time embedding shows a significant advantage for participants A03 (12.5% improvement) and A04 (16.7% improvement). For the ConvNet architecture, the most notable improvement was observed in participant A06 (7.3% improvement).

The results from the Wilcoxon signed-rank test indicate

significant differences between the ConvNet and EEGNet architectures. In the BCI4-2A dataset, ConvNet exhibited significant performance improvements with the traveling-wave based time embedding strategy ($P < 0.05$), whereas EEGNet did not show significant differences ($P > 0.05$).

4.2 Results for BCI4-2B dataset

The BCI4-2B dataset employed the same analysis methods as BCI4-2A. From Table 2, traveling-wave based time embedding also proved to be beneficial. For example, the average classification accuracy of ConvNet with the hyperparameters $t=125$, $\lambda=4,000$ is 82.6%, while the average classification accuracy of ConvNet without time embedding is 81.8%. For the EEGNet, the optimal hyperparameter combination $t=250$, $\lambda=4,000$ yielded an average classification accuracy of 85.5% in BCI4-2B. Similarly, compared to position encoding in Transformer, traveling-wave embedding generally showed better classification performance for most participants in BCI4-2B. The time embedding strategy also demonstrated variations among participants and differences in neural network architecture responses. Notably, although the benchmark architectures of ConvNet and EEGNet performed differently compared to BCI4-2A, their responses to the time embedding

strategy also varied from BCI4-2A. The results from the Wilcoxon signed-rank test reveal that ConvNet did not exhibit significant changes with the travelling-wave based time embedding strategy ($P > 0.05$), whereas EEGNet showed significant changes ($P < 0.05$). Regardless of the architecture, whether ConvNet or EEGNet, the classification performance of participants B02 and B03 was significantly enhanced. Compared to other participants, B02 and B03 are often referred to as “EEG-illiteracy” because their EEG signals are typically harder to decode.

4.3 Impact of hyperparameter variations on participant decoding accuracy

To comprehensively examine the effects of hyperparameter values in traveling-wave based time embedding on decoding accuracy across different participants, Fig. 4 presents violin plots that illustrate the variability in decoding accuracy with different hyperparameter combinations compared to a benchmark network architecture. The values for t in the traveling-wave based time embedding were explored within the set $\{0, 125, 250, 375, 500\}$, and for λ within $\{4\,000, 8\,000, 12\,000, 16\,000, 1\,000\,000\}$, resulting in 25 experimental outcomes for each participant across each network architecture. Fig. 4 vividly captures the variations in decoding accuracy post-time embedding, as well as the differential impacts of various decoding networks and electrode datasets on the performance of time embedding.

A “tall and slim” violin plot indicates that a participant is particularly sensitive to the hyperparameter values, whereas a “short and wide” violin plot suggests a lower sensitivity. Fig. 4 also reveals that some participants, such as B02 and B03, experience significant improvements in decoding performance following the application of time embedding. However, not all participants benefit from the time embedding strategy. For example, participants A05 and B06 show a decrease in decoding performance after the application of time embedding. The majority of participants’ decoding outcomes depend on the choice of hyperparameters in the time embedding, and selecting appropriate hyperparameter combinations can substantially enhance decoding performance for these individuals.

4.4 Hyperparameter analysis in traveling-wave based time

As depicted in Fig. 4, the application of traveling-wave based time embedding resulted in improved

decoding accuracy for some participants, while others experienced a decrease. Consequently, Fig. 5 examines the generalizability of traveling-wave based time embedding across different network architectures. The heatmap in Fig. 5 uses a zero baseline, representing the average accuracy across all participants for the benchmark within the dataset. This visualization demonstrates that the ConvNet architecture exhibits greater robustness compared to EEGNet, evidenced by smaller fluctuations in average accuracy across the dataset under varying hyperparameter settings of traveling-wave based time embedding.

On the other hand, compared to the results in Tables 1 and 2, the overall increase in average accuracy across the dataset is modest, suggesting that different participants have distinct preferences for the hyperparameters in time embedding. This indirectly supports the variability in temporal preferences among participants during motor imagery. For ConvNet, a robust hyperparameter combination is $\lambda = 4\,000$ and $t = 375$, which consistently improved average accuracy across two different datasets. In contrast, for EEGNet, an increase in λ to $1\,000\,000$ generally led to a decline in average accuracy across various combinations, indicating limited recognition capabilities for position encoding. This may relate to EEGNet’s network architecture, which features sparse connections and a spatial convolution followed by an additional temporal convolution layer.

5 Conclusions

This study has examined the efficacy of time embedding methods in the context of MI-EEG decoding, with a particular focus on a novel traveling-wave based time embedding approach integrated as a pseudo channel into MI-EEG signals. Extensive validations were carried out in two influential artificial neural network architectures and two datasets with significant variations in the number of channels. The experimental results confirm that the traveling-wave based time embedding method significantly enhances decoding accuracy, especially when optimal hyperparameters are selected. This improvement is especially pronounced in specific subsets of participants, especially for some participants who are considered as “EEG-illiteracy”. Moreover, this method outperforms the position encoding method used in Transformer architecture in terms of performance and robustness across diverse network architectures and motor imagery datasets.

However, the traveling-wave based time embedding model proposed in this study is a single-peak model, and only a limited 5×5 hyperparameter search was conducted for the parameters. The effectiveness of time embedding in MI-EEG was solely evaluated based on decoding accuracy, which significantly limits its application in enhancing the interpretability of EEG data. Future research will focus on two main directions: 1) exploring the underlying neural mechanisms of the optimal time embedding model from perspectives such as time-frequency analysis and participant attention mechanisms; 2) investigating the impact of time embedding, when integrated as a pseudo-channel into EEG signals, on the feature extraction process of artificial neural networks, with an emphasis on model interpretability.

Acknowledgement

This work was supported in part by Ernst-Mach scholarship. We extend our gratitude to Yiwei Yang for polishing the Figures.

Declaration of conflicting interests

The authors declare that they have no known competing financial interests or personal relationships that could have appeared to influence the work reported in this paper.

References

- [1] WOLPAW J R, BIRBAUMER N, MCFARLAND D J, et al. Brain-computer interfaces for communication and control. *Clinical Neurophysiology*, 2002, 113(6): 767-791.
- [2] PFURTSCHELLER G, NEUPER C. Motor imagery and direct brain-computer communication. *Proceedings of the IEEE*, 2001, 89(7): 1123-1134.
- [3] PFURTSCHELLER G, BRUNNER C, SCHLOGL A, et al. Mu rhythm (de) synchronization and EEG single-trial classification of different motor imagery tasks. *NeuroImage*, 2006, 31(1): 153-159.
- [4] HOCHBERG L R, BACHER D, JAROSIEWICZ B, et al. Reach and grasp by people with tetraplegia using a neurally controlled robotic arm. *Nature*, 2012, 485(7398): 372-375.
- [5] LAZAROU I, NIKOLOPOULOS S, PETRANTONAKIS P C, et al. EEG-based brain-computer interfaces for communication and rehabilitation of people with motor impairment: a novel approach of the 21 st century. *Frontiers in Human Neuroscience*, 2018, 12. DOI:10.3389/fnhum.2018.00014.
- [6] ANTONENKO P, PAAS F, GRABNER R, et al. Using electroencephalography to measure cognitive load. *Educational Psychology review*, 2010, 22: 425-438.
- [7] CHO H, AHN M, AHN S, et al. EEG datasets for motor imagery brain-computer interface. *GigaScience*, 2017, 6(7): 1-8.
- [8] KAYA M, BINLI M K, OZBAY E, et al. A large electroencephalographic motor imagery dataset for electroencephalographic brain computer interfaces. *Scientific Data*, 2018, 5(1): 180211.
- [9] TANGERMAN M, MULLER K-R, AERTSEN A, et al. Review of the BCI competition IV. *Frontiers in Neuroscience*, 2012, 6: 5501-5513.
- [10] ANG K K, CHIN Z Y, ZHANG H H, et al. Filter bank common spatial pattern (FBCSP) in brain-computer interface//2008 IEEE International Joint Conference on Neural Networks (IEEE World Congress on Computational Intelligence), June 1-8, 2008, Hong Kong, China. New York: IEEE, 2008: 2390-2397.
- [11] MIAO Z Q, ZHAO M R. Weight freezing: a regularization approach for fully connected layers with an application in EEG classification. 2023: 2306.05775. <http://arxiv.org/abs/2306.05775v2>
- [12] SCHIRMEISTER R T, SPRINGENBERG J T, FIEDERER L D J, et al. Deep learning with convolutional neural networks for EEG decoding and visualization. *Human Brain Mapping*, 2017, 38(11): 5391-5420.
- [13] LAWHERN V J, SOLON A J, WAYTOWICH N R, et al. EEGNet: a compact convolutional neural network for EEG-based brain-computer interfaces. *Journal of Neural Engineering*, 2018, 15(5): 056013.
- [14] AFLALO T, KELLIS S, KLAES C, et al. Neurophysiology. Decoding motor imagery from the posterior parietal cortex of a tetraplegic human. *Science*, 2015, 348(6237): 906-910.
- [15] MIAO Z Q, ZHAO M R, ZHANG X, et al. LMDA-Net: a lightweight multi-dimensional attention network for general EEG-based brain-computer interfaces and interpretability. *NeuroImage*, 2023, 276: 120209.
- [16] VASWANI A, SHAZEER N, PARMAR N, et al. Attention is all you need. *Advances in Neural Information Processing Systems*, 2017: 5998-6008.
- [17] WU K, PENG H W, CHEN M H, et al. Rethinking and improving relative position encoding for vision transformer//2021 IEEE/CVF International Conference on Computer Vision, October 10-17, Montreal, Q C, Canada. New York: IEEE, 2021: 10013-10021.
- [18] SHIV V, QUIRK C. Novel positional encodings to enable tree-based transformers//33rd Conference on Neural Information Processing Systems (NeurIPS 2019), December 9-15, 2019, Vancouver, Canada. Neural Information Processing Systems Foundation, 2019.
- [19] ISLAM M A, JIA S, BRUCE N D B. How much position information do convolutional neural networks encode? 2020: 2001.08248. <http://arxiv.org/abs/2001.08248v1>.
- [20] JEUNET C, JAHANPOUR E, LOTTE F. Why standard brain-computer interface (BCI) training protocols

- should be changed: an experimental study. *Journal of Neural Engineering*, 2016, 13(3): 036024.
- [21] BCI4-2A dataset. [2024-07-21]. <https://www.bbc.de/competition/iv/#dataset2a>.
- [22] BCI4-2B dataset. [2024-07-21]. <https://www.bbc.de/competition/iv/#dataset2b>.
- [23] MIAO Z Q, ZHAO M R. Time-space-frequency feature Fusion for 3-channel motor imagery classification. *Biomedical Signal Processing and Control*, 2024, 90: 105867.
- [24] MIAO Z Q, ZHANG X, MENON C, *et al.* Priming cross-session motor imagery classification with A universal deep domain adaptation framework. *Neurocomputing*, 2023, 556: 126659.

伪导联:用于运动想象解码的时间嵌入方法

苗政清^{1,2*}, 赵美蓉¹

1. 天津大学 精密测试技术与仪器国家重点实验室, 天津 300072;
2. 维也纳大学 计算机科学学院神经信息学研究团队, 维也纳 1090, 奥地利

摘要: 基于运动想象(Motor imagery, MI)的脑电图(Electroencephalogram, EEG)研究在实现外部设备的神经控制和神经康复方面处于前沿地位。本研究提出了一种新颖的时间嵌入技术,称为基于行波的时间嵌入,并将其作为伪通道用于增强多种神经网络架构中MI-EEG信号的解码精度。与传统神经网络方法无法考虑个体差异的时间动态性不同,我们的方法基于先验知识捕捉了不同参与者的时间相关变化。通过对多名参与者的实验表明,该方法不仅提高了分类准确性,而且在适应个体差异方面优于Transformer架构中的位置编码。研究结果显示,基于行波的时间嵌入显著提高了那些通常被认为是“脑电文盲”参与者的解码精度。作为EEG研究的新方向,基于行波的时间嵌入不仅为神经网络解码策略提供了新的见解,还为神经科学中的注意力机制研究和对EEG信号的深入理解开辟了新的研究途径。

关键词: 运动想象; 伪通道; 脑电图; 神经网络

引用格式: MIAO Zhengqing, ZHAO Meirong. Pseudo channel: time embedding for motor imagery decoding. *Journal of Measurement Science and Instrumentation*, 2024, 15(3): 308-317.